Scientific Research Publishing

Open Journal of Applied Sciences, 2025, 15(1), 202-219
https://www.scirp.org/journal/ojapps
ISSN Online: 2165-3925
ISSN Print: 2165-3917

Modeling the Cardiovascular System for the Simulation of Special Cases of Pulmonary Hypertension

Jefferson Sidoine Tadjonang Tegne[1], René Thierry Djoumessi[1,2], François Beceau Pelap[1]

[1]UR de Mécanique et de Modélisation des Systèmes Physiques (UR-2MSP), Département de Physique, Faculté des Sciences, Université de Dschang, Dschang, Cameroon
[2]IMT School for Advanced Studies Lucca, MUSAM, Lucca, Italy
Email: renethierrydjoumessi@yahoo.com, tadjonangjefferson@gmail.com, fbpelap@yahoo.fr, francois.pelap@univ-dschang.org

How to cite this paper: Tadjonang Tegne, J.S., Djoumessi, R.T. and Pelap, F.B. (2025) Modeling the Cardiovascular System for the Simulation of Special Cases of Pulmonary Hypertension. *Open Journal of Applied Sciences*, **15**, 202-219.
https://doi.org/10.4236/ojapps.2025.151014

Received: December 9, 2024
Accepted: January 23, 2025
Published: January 26, 2025

Copyright © 2025 by author(s) and Scientific Research Publishing Inc.
This work is licensed under the Creative Commons Attribution International License (CC BY 4.0).
http://creativecommons.org/licenses/by/4.0/

Open Access

Abstract

This study examines hemodynamic behavior in particular cases of pulmonary hypertension without treatment. Pulmonary hypertension represents an anomalous hemodynamic state and is characterized by an excessively high blood pressure in the pulmonary artery. To simulate the hemodynamic abnormalities in pulmonary hypertension under different causes and pathologies, we construct a localized parameter circuit model governed by nonlinear ordinary derivative equations of the human circulatory system. Thus, two special cases are considered, namely pulmonary the artery stenosis and the left ventricular diastolic dysfunction. For each case of pulmonary hypertension development, we determine the relationships between blood pressure and chamber and vessel pressure-volume. When the pulmonary hypertension is due to pulmonary artery stenosis, it appears that the right ventricular pressure increases up to 90 mm Hg, likewise the rise in pulmonary artery resistance induces direct increment in pulmonary artery pressure. However, when the pulmonary hypertension is due to left ventricular diastolic dysfunction, we note that the left atrial pressure and the pulmonary vein pressure augment, leading to the growth of the pulmonary artery blood pressure. The established results within this paper are useful for understanding the hemodynamic mechanism of particular pulmonary hypertension.

Keywords

Pulmonary Hypertension, Hemodynamic Modeling, Pulmonary Artery Stenosis, Left Ventricular Diastolic Dysfunction

1. Introduction

Pulmonary hypertension (PHT) is defined as a mean pulmonary arterial pressure greater or equal to 25 mm Hg at rest and encompasses five main causes, all of which lead to heart failure if untreated [1]. The World Health Organization defines five classes of PHT based on different causes [2]. Regardless of the class of which the patient belongs, PHT is a serious condition. If PHT is not detected and treated early, pulmonary artery pressure will rise to systemic levels and right ventricular heart failure becomes inevitable [3]. Since any PHT class can be defined by abnormal hemodynamics in the right heart and lungs, it is necessary to understand time course of hemodynamic changes. Currently, the gold standard procedure for the diagnosis and evaluation of PHT remains the right heart catheterization which directly determines blood pressure in the right heart and lungs [4]. Due to the existence of many interactions within the cardiovascular system, it becomes difficult to evaluate how little change in one cardiac or vascular parameter could affect the overall hemodynamics of the patient. However, several mathematical models and numerical simulations have been proposed to understand the causes and development of abnormal hemodynamics in the systemic and pulmonary circulation system. Therefore, Analog circuit models constructed for heart failure revealed a decrease in left ventricular blood pressure and cardiac output, with a significant change in the left ventricular pressure-volume loop [5] [6]. Furthermore, Korurek *et al.* [7] modelled severe aortic valve stenosis by raising the value of aortic valve resistance in the analog circuit model. They obtained a significant elevation of left ventricle (LV) systolic blood pressure and mean aortic pressure gradient, as well as a decrease in aortic systolic blood pressure.

On the other hand, mitral stenosis [8], mitral regurgitation and aortic regurgitation [9] that cause hemodynamic abnormalities in the cardiovascular system were also studied through numerical models. Luo *et al.* [10] examined two causes leading to left ventricular diastolic dysfunction (LVDD). They modeled the impaired left ventricular active relaxation by altering the activation function of the LV and, the increase in passive stiffness by increasing the diastolic stiffness of LV wall and septum. Their results showed that abnormal LV diastolic performance alone can lead to decreasing of LV and right ventricle (RV) systolic performance [10]. Furthermore, Korurek *et al.* [11] simulated Eisenmenger syndrome with a ventricular septal defect. They found a remarkable growth in RV pressure and pulmonary artery pressure, but observed a weakening in LV pressure, aortic pressure, aortic flow and pulmonary compliance.

In this paper, a lumped parameter model of the cardiopulmonary system to simulate two particular cases of PHT is proposed. Indeed, most of the existing works in the literature related to the study of this pathology are more clinical studies [12] [13], with the exception of the work of Hong *et al.* [14] dealing with an analytical investigation thanks to their lumped parameter model proposed to examine the behavior of four particular cases of PHT on the cardiovascular system. Based on the model developed by Hong *et al.* [14], we propose a model that allows

us to study the behavior of the cardiovascular system during the development of PHT.

The organization of this paper is structured as follows. In Section 2, the scientific methodology usually called to study pathologies related to PHT is presented. In Section 3, we exhibit results established from different simulations carried out for each pathology dealing with PHT. Section 4 is devoted to discussion of the obtained results and comparison with existing works for their validation. In Section 5, concluding remarks and some limitations of the work are given.

2. Methods

Previous studies showed a general equivalence between the blood flow in the circulation system and the current flow in an analog circuit [14] [15]. Blood pressure and blood flow are equivalent to voltage and charge flow. The resistance of blood flow is equivalent to the electronic resistance. The inertia of the blood flow is modeled by the inductance. The entry and exit of blood into the vessel is similar to the charging and discharging of a linear or nonlinear capacitor. The pumping of blood into a heart chamber can be simulated by a voltage source that is nonlinear with respect to volume and time. Therefore, an analog circuit model for the human circulation system proposed by Ursino [16] is taken as a starting point to simulate two typical PHT cases (**Figure 1**).

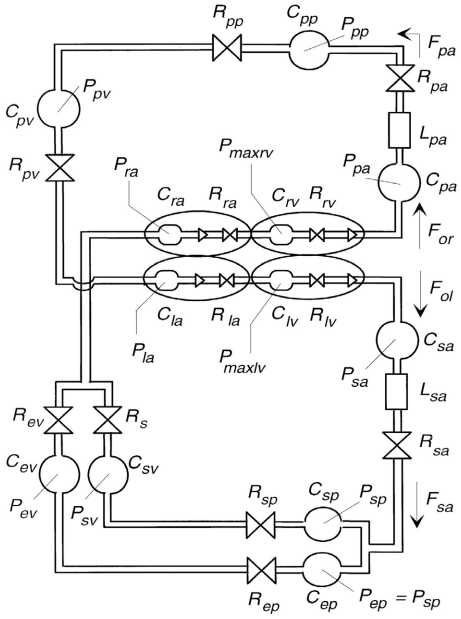

Figure 1. Hydraulic analog of cardiovascular system using the lumped parameter model [16].

In **Figure 1**, the capital letters have the following meaning: P is the pressure, R represents the hydraulic resistance, C defines the compliance, L stands for the inductance and F designates the flow rate. The different components of the system are identified by particular subscript abbreviations in order to simplify the

understanding of the model equations (Table 1).

Table 1. Parameters that describe the hydraulic analogue of the cardiovascular system.

Subscripts	Significations	Subscripts	Significations
pa	pulmonary arteries	pp	pulmonary peripheral
pv	pulmonary veins	sa	systemic arteries
sp	systemic peripheral	ev	Extra-splanchnic venous
sv	splanchnic venous	ep	Extra-splanchnic peripheral
ra	right atrium	la	left atrium
rv	right ventricle	lv	left ventricle
i	In	o	Out
l	Left	r	Right

A segment analogy is adopted to design a model of the cardiovascular system. With this method, the cardiovascular system is considered as a sequence of interconnected elastic segments likened to reservoirs full of blood. Each segment is described at each instant by a pressure $P(t)$ acting on the segment wall, a volume $V(t)$ it contains, an inflow $Q_i(t)$ and outflow $Q_o(t)$. The diagram of the elastic chamber is depicted in Figure 2. According to the conservation of mass, the main equation of volume in each elastic segment is summarized as follows:

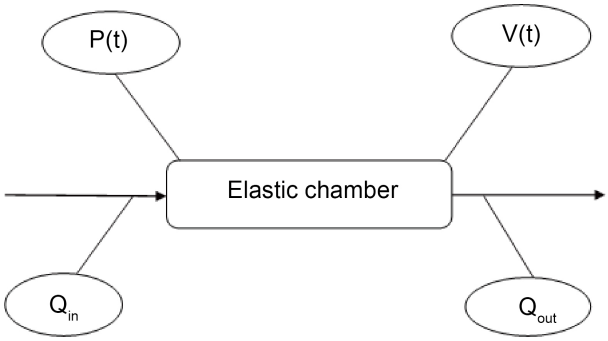

Figure 2. Elastic chamber of the cardiovascular system. Q_{in} and Q_{out} represent, respectively, the blood flow rate in, and flow rate out; $P(t)$ and $V(t)$ designate, respectively, the pressure and volume of the elastic chamber.

$$\frac{\mathrm{d}V(t)}{\mathrm{d}t} = Q_i(t) - Q_o(t) \tag{1}$$

To assess the pressure in each segment, we consider the assumption made by Frolov *et al.* [17] that is, the more blood in the segment, the more wall deformation and therefore the more pressure in the segment. This correlation is defined by equation:

$$P(t) = \frac{1}{C}\left(V(t) - V_0\right) \tag{2}$$

Following the same approach, the blood flow rate between two linked segments is defined by Poiseuille's law [18]:

$$\frac{\mathrm{d}Q(t)}{\mathrm{d}t} = \rho\left(P_i(t) - P_o(t)\right) \tag{3}$$

The heart is constituted of four chambers: the left ventricle, the left atrium, the right ventricle and the right atrium. The left and right atria are passive organs, as they do not contribute to the contractile activity of the heart. Therefore, Equations (1-2) are applied to characterize the left and right ventricles.

2.1. PHT Due to Pulmonary Artery Stenosis

Blood flows more easily through the vessels when the pulmonary arteries are healthy and flexible. The synergistic effects of pulmonary vascular remodeling, vasoconstriction, and *in situ* thrombosis lead to an increase in pulmonary vascular resistance (PVR) and result in PHT [15]. However, the elevation of pulmonary artery pressure caused by pulmonary vasoconstriction is reversible in the early stage of PHT. Moreover, the development of stenosis, thickening of the intima and medial membrane, lead to irreversible changes in vascular structure. Furthermore, the compact and rigid walls of the arteries limit blood flow and increase resistance. As the artery narrows further, blood flow is restricted. Pulmonary vascular remodeling is the major pathological change in PHT [15].

Now, we consider the pulmonary arteries and establish the nonlinear relationship between pressure and volume. Owing to the Poiseuille's law, the fluid flow rate Q is given by the following relationship:

$$Q = \pi(\Delta P) r^4 / 8\mu l \tag{4}$$

where r is the radius, ΔP is the pressure difference, l is the length of the pipe, and μ is the viscosity of the liquid. We assume that that l and μ are constants. The quantity Q is proportional to ΔP and inversely proportional to the blood flow resistance R, explained by the Ohm's law:

$$Q = \Delta P / R \tag{5}$$

Then it appears that the resistance to blood flow R is inversely proportional to the fourth power of r *i.e.*,

$$R = 8\mu l / \pi r^4 \tag{6}$$

In order to simulate the development of pulmonary artery and proximal pulmonary artery narrowing over time, the radius decreases as a function of time according to the relationship [15]:

$$r(t) = r_0\left(1 + g_0 * t\right)^{-1/4} \tag{7}$$

in which r_0 is the initial radius and g_0 is used for the rate of progression (**Table 2**). Clinical observations showed that resistance develops slowly and its progression may take years [19]. Therefore, it is reasonable to assume that the artery with stenosis does not undergo any short-term changes. In this case, the artery

could be in an equilibrium state in a short time and Poiseuille's law is thus validated. The short time in this study is assumed to correspond to the duration of a single cardiac cycle. Hence, it could be assumed that the artery undergoes no change during a cardiac cycle. This study simulates pulmonary artery stenosis (PAS) with these hypotheses and the relationships between the resistance of pulmonary arteries (R_{pa}), the resistance of peripheral pulmonary (R_{pp}) and r are given as follows:

Table 2. Values of the diverse parameters in the model of PAS.

Parameters	Values	Parameters	Values
$R_{pa,0}$	0.023	k_{10}	0.0013
$R_{pp,0}$	0.0894	σ	0.0008
$E_{es-rv,0}$	2.1 mm Hg/mL	r_0	0.6
τ_0	0.35 S	g_0	0.018
V_{pa}	123 ml	V_{pp}	123 ml

$$R_{pa}\left(r(t),t\right)=\left(1/r(t)\right)^4 * R_{pa,0} \tag{8a}$$

$$R_{pp}\left(r(t),t\right)=\left(1/r(t)\right)^4 * R_{pp,0} \tag{8b}$$

where $R_{pa,0}$ and $R_{pp,0}$ are the initial values of R_{pa} and R_{pp}. Previous studies [20] [21] have shown that the resistance R and the compliance C are inversely related. However, recent evidence suggests that this concept should be revisited [22], their product decreases as normalized pulmonary vascular stiffness increases. In this study, we accept the new finding that the product of R and C, named RC-time, decreases with time:

$$R * C = \tau(t) \tag{9a}$$

$$\tau(t)=\tau_0 * \mathrm{e}^{-\sigma t} \tag{9b}$$

in which τ_0 is the initial value of RC-time in the normal heart, and σ is a parameter to control the rate of change (**Table 2**). Hence, the compliance of the pulmonary artery (C_{pa}) and that of the proximal pulmonary artery (C_{pp}) are defined by:

$$C_{pa}\left(r(t),t\right)=\tau(t)r^4(t)/R_{pa,0} \tag{10a}$$

$$C_{pp}\left(r(t),t\right)=\tau(t)r^4(t)/R_{pp,0} \tag{10b}$$

Based on the pressure-volume relationship, one deduces from Equations (10) the expressions of the pressures of the pulmonary artery and that of the proximal pulmonary artery, respectively:

$$P_{pa}=\frac{V_{pa} * R_{pa,0}}{\tau(t) * r^4(t)} \tag{11a}$$

$$P_{pp} = \frac{V_{pp} * R_{pp,0}}{\tau(t) * r^4(t)} \tag{11b}$$

in which V_{pa} and V_{pp} are, respectively, the volume of the pulmonary artery and that of the proximal pulmonary artery.

With the progression of PAS, the PVR afterload, and the mean pulmonary artery pressure ($mPAP$) may progressively increase [23]. In this case, the RV hypertrophy can be reformed by raising the thickness and contractility of the ventricular wall to accommodate the continuous rise in $mPAP$. In this paper, compensation of the RV to accommodate the continuous rise in $mPAP$ is achieved by raising the end-systolic elastance of the right ventricle (E_{es-rv}) according to the relationship:

$$E_{es-rv}(t) = E_{es-rv,0} + k_{10} * t \tag{12}$$

where k_{10} is the rate-of-change control parameter and $E_{es-rv,0}$ is the initial value of E_{es-rv} (**Table 2**).

2.2. PHT Caused by Left Ventricular Diastolic Dysfunction

2.2.1. Ventricular Model

In accordance with Sagawa *et al.* [24], we consider that the isometric pressure-volume relationship is exponential at end-diastole when the ventricle is relaxed and, linear at end-systole when the ventricle is in maximal contraction. The end-diastolic and end-systolic pressure-volume functions of the ventricle are then determined by:

$$P_{ES} = E(V_{ES} - V_0) \tag{13}$$

$$P_{ED} = B\exp\lfloor A(V_{ED} - V_0)\rfloor - B \tag{14}$$

where E represents the end-systolic elastance of the ventricle, V_0 is the associated ventricle unconstrained volume, B and A are coefficients characterizing the exponential form of the end-diastolic pressure-volume relationship (EDPVR). The latest are obtained by integrating the time-evolving ventricular activation function $0 < \varphi(t) < 1$ (with $\varphi(t) = 0$ at maximum contraction and $\varphi(t) = 1$ at complete relaxation) and admitting that $V_{lv} = V_{ES} = V_{ED}$ at the beginning of the cardiac cycle. Therefore, when the ventricle is maximally contracted, we have:

$$P_{max,lv} = \varphi(t)P_{ED} + (1 - \varphi(t))P_{ED} \tag{15}$$

Hence, the ventricle mechanic model is defined by:

$$\begin{aligned} P_{max,lv} = {} & \varphi(t)E_{lv}(V_{lv} - V_{lv,0}) \\ & + (1 - \varphi(t))\left(B_{lv}\exp\lfloor A_{lv}(V_{lv} - V_{lv,0})\rfloor - B_{lv}\right) \end{aligned} \tag{16}$$

All parameters exploited for simulating the dynamics of the mechanical models of the ventricle are given in **Table 3**.

Table 3. Parameters of the LV mechanical models.

Parameters	Values
E_{lv}	3.1 mm Hg/mL
$V_{lv,0}$	40 mL
$B_{lv,0}$	1.7 mm Hg
$A_{lv,0}$	0.015 mL^{-1}
$K_{e,lv}$	0.000475 S/mL

2.2.2. Introduction of PHT

The LV pressure-volume loop is the most direct manifestation of hemodynamic abnormalities. Previous researchers have shown that, the EDPVR moves upward in the LVDD [25], which is an exponential function controlled by A_{lv} and B_{lv}. In order to simulate LVDD pathology, it is necessary to increase the values of A_{lv} and B_{lv} with respect to time to increase the LV diastolic pressure, therefore:

$$A_{lv}(t) = A_{lv,0} + K_{11} * t \tag{17}$$

$$B_{lv}(t) = B_{lv,0} + K_{22} * t \tag{18}$$

where K_{11} and K_{22} are the coefficients, $A_{lv,0}$ and $B_{lv,0}$ are the initial values of A_{lv} and B_{lv} defined in **Table 4**. To simulate the development of PHT in this case, the EDPVR defined by (16) becomes:

$$\begin{aligned} P_{max,lv} = {} & \varphi(t) E_{lv}\left(V_{lv} - V_{lv,0}\right) \\ & + \left(1-\varphi(t)\right)\left(B_{lv}(t)\exp\left\lfloor A_{lv}(t)\left(V_{lv} - V_{lv,0}\right)\right\rfloor - B_{lv}(t)\right) \end{aligned} \tag{19}$$

Table 4. Parameters for the simulation of LVDD.

Parameters	Value
$E_{es-rv,0}$	1.7 mmHg/mL
K_{11}	0.0035
K_{22}	0.000075
K_{33}	0.7

This PHT is strongly linked to the RV. The concept of integration of the RV and the pulmonary circulation have been proposed by Noordegraaf *et al.* [26]. Under normal physiological conditions, the RV is sensitive to elevated pressure. Indeed, it is connected to the pulmonary circulation at low pressure, low resistance, and high compliance. In the early stage of PHT, the RV dynamics will try to compensate the elevated pulmonary artery pressure. With the development of the disease, in order to adapt to the continuous rise in afterload and maintain ejection capacity, the RV enlarges until right heart failure eventually occurs. Acosta *et al.* [22] attempted unsuccessfully to definitively resolve this RV failure.

With the development of this type of PHT, the RV in the LVDD model overcomes the elevation of afterload by elevating myocardial contractility E_{es-rv} which is given as follows:

$$E_{es-rv}(t) = E_{es-rv,0} + K_{33} * t \tag{20}$$

where K_{33} is the rate of change control parameter, $E_{es-rv,0}$ is the initial value of E_{es-rv} (Table 4).

3. Results

We implement this model in Matlab as a series of differential equations using the forth order Runge-Kutta algorithm for the volume changes of each segment. The simulation time is set to 20 s, and the cardiac cycle to 0.8s. We use a time step of 1ms in the numerical solution. An 8 GB RAM, 64-bit operating system, and 2.4 GHz Intel Core i5-3770 running MATLAB 2015b ran all simulations. We assume that the time-varying parameters do not vary during a cardiac cycle and but could increase or decrease between adjacent cycles.

Figure 3 displays the Pressure-Volume loops of two heart chambers for normal state and simulated hemodynamics of two cardiac cycles. Figure 3(a) shows the relationship between the left and right ventricular pressure and volume. It appears that the left ventricular pressure reaches 120 mmHg while the maximal value of the RV pressure remains under 25 mmHg.

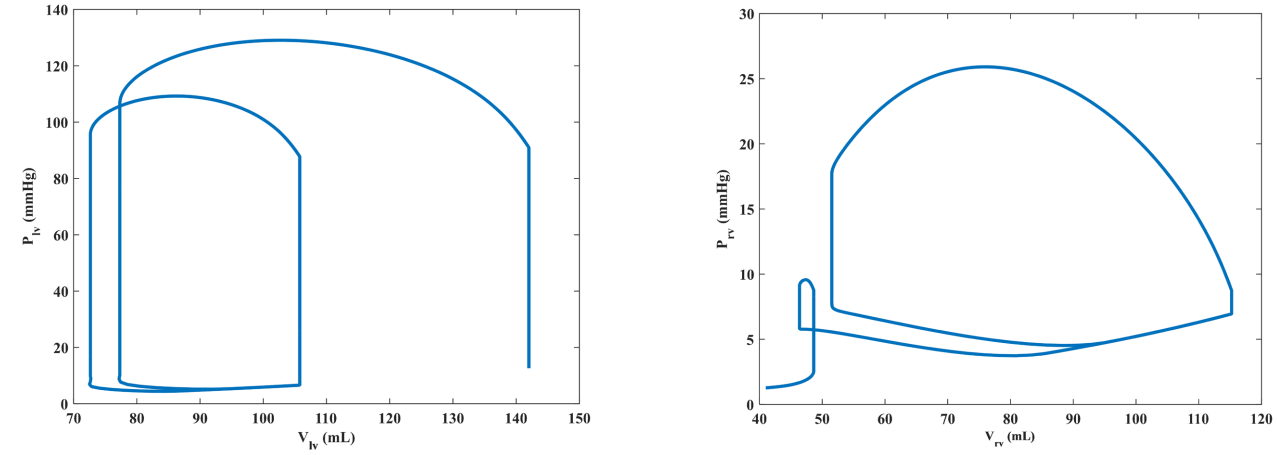

(a)

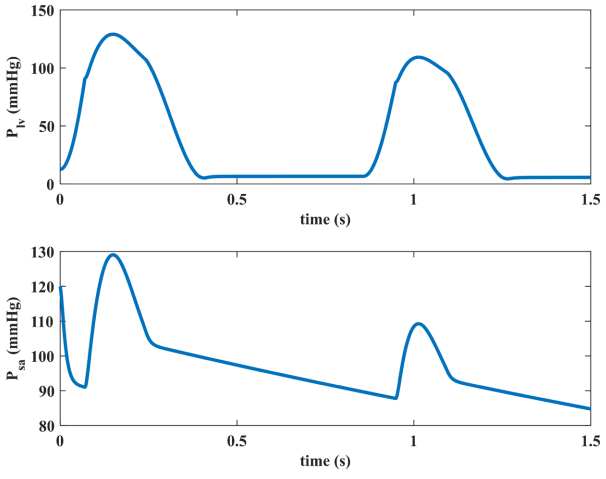

(b)

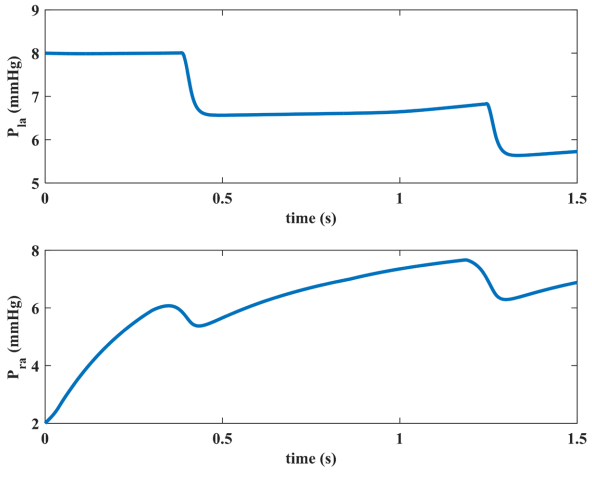

(c)

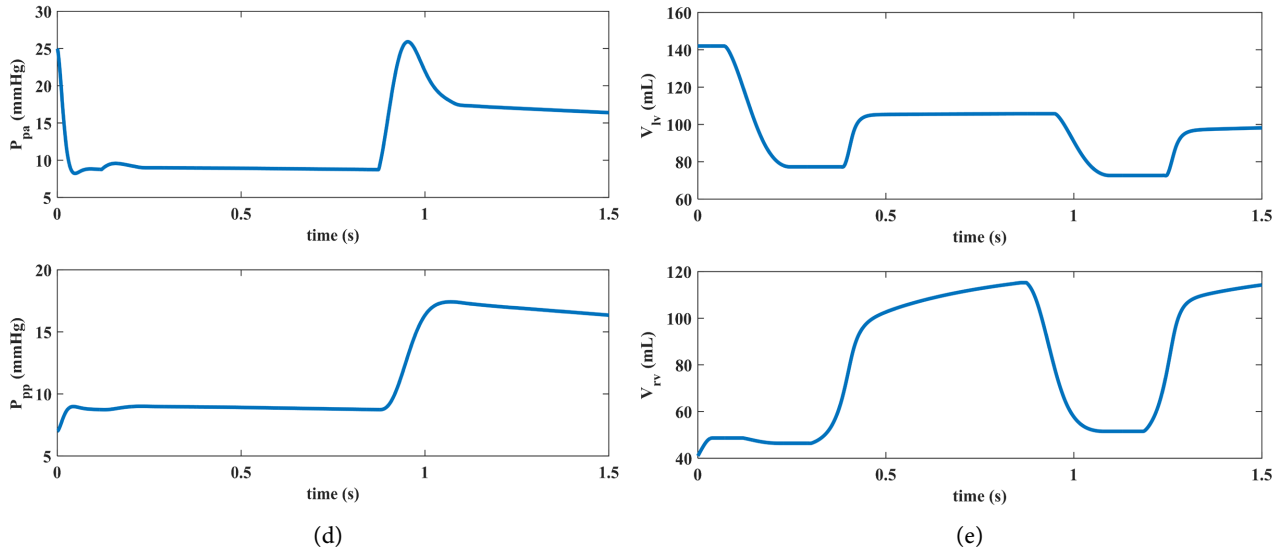

(d) (e)

Figure 3. Pressure-Volume (P-V) loops of two heart chambers for normal state and simulated hemodynamics of two cardiac cycles. (a): P-V loops of LV and RV; (b): The pressure signals in LV and systemic peripheral; (c): The pressure signals in left atrium and right atrium; (d): The pressure signals in pulmonary arteries and pulmonary peripheral; (e) The volume signals in LV and RV.

Figure 3(b) exhibits temporal behavior of left ventricular pressure and peripheral systemic pressure. One observes from these plots that variation in left ventricular pressure is lower than that of the peripheral systemic pressure. These results corroborate those established by Ursino [16]. It appears from **Figure 3(c)** that the left atrial pressure decreases with time while that of the right atrium increases. **Figure 3(d)** reveals that pulmonary artery pressure is always greater than the peripheral pulmonary pressure while **Figure 3(e)** allows observing that the amplitude of variation of left ventricular volume is lower than that of the right ventricular volume.

3.1. Results of PHT Caused by Pulmonary Artery Stenosis

The pathological mechanism in PHT simulation allows for changes in pulmonary artery resistances over time. **Figure 4** displays the pressure-volume loops of two heart chambers for PHT due to the PAS. The blue curves describe normal healthy (normal) situation clearly shown in **Figure 3(a)** while the orange curves deal with pathological conditions (case with PHT). Comparing these results with normal hemodynamic conditions, it becomes relevant to note that the systolic blood pressure of the RV rises over 25 mmHg until it reaches 90 mmHg. Similarly, the rise in pulmonary artery pressure is high enough to shift forward the blood flow in the pulmonary circulation. These results corroborate with those established by Lock *et al.* [27].

Now, we check the development of the key pulmonary blood pressures and volume for PHT due to PAS. We focus on temporal evolution of pressure and volume signals in the pulmonary arteries and pulmonary peripheral. The obtained results are plotted in **Figure 5**. The graphs of **Figure 5(a)** exhibit the dynamics of pulmonary artery pressure (Ppa) and peripheral pulmonary pressure (Ppp) showing that

increase in pulmonary artery resistance directly causes an increase in pulmonary artery blood pressure. The same observations are made in the peripheral pulmonary artery (orange curves). On the other hand, **Figure 5(b)** presents the temporal evolution of the pressure and volume signals in the right ventricular. Let us note that during PHT, right ventricular pressure rises leading to a growth of the right ventricular volume (orange).

These results dealing with our model are consistent with previous clinical observations. Indeed, Lock *et al*. [27] examined children with right and left pulmonary artery stenosis (or hypoplasia) and established that their right ventricular pressure increases to 105.3 ± 37.4 (mean ± SD) mmHg in pre-dilation and

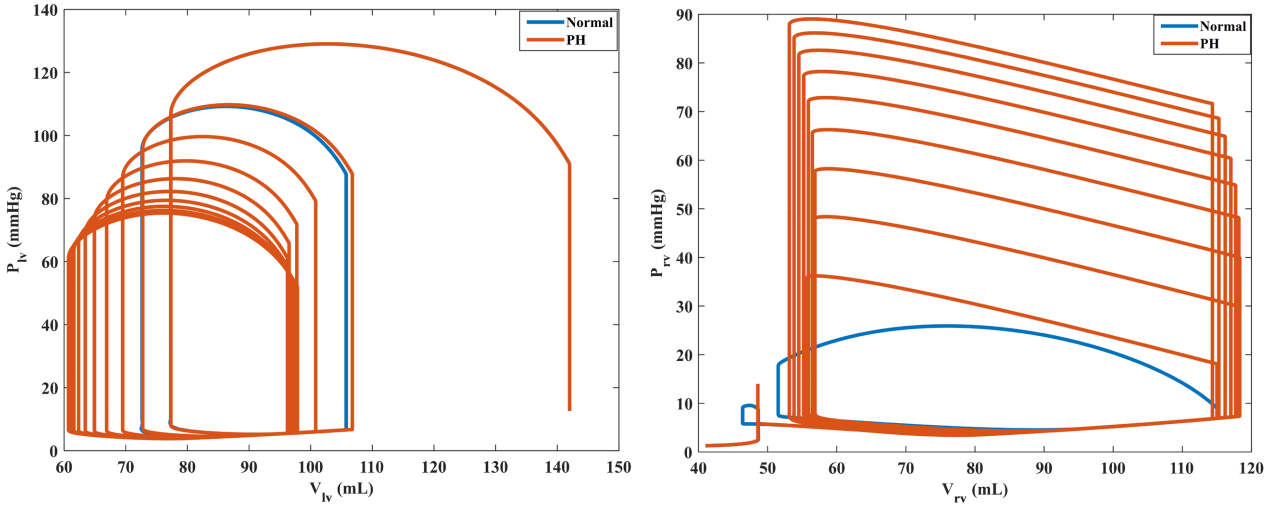

Figure 4. P-V loops of two chambers for PHT due to PAS. The loops blue are normal and the orange ones are for developing PHT. (a): P-V loops of LV; (b): P-V loops of RV.

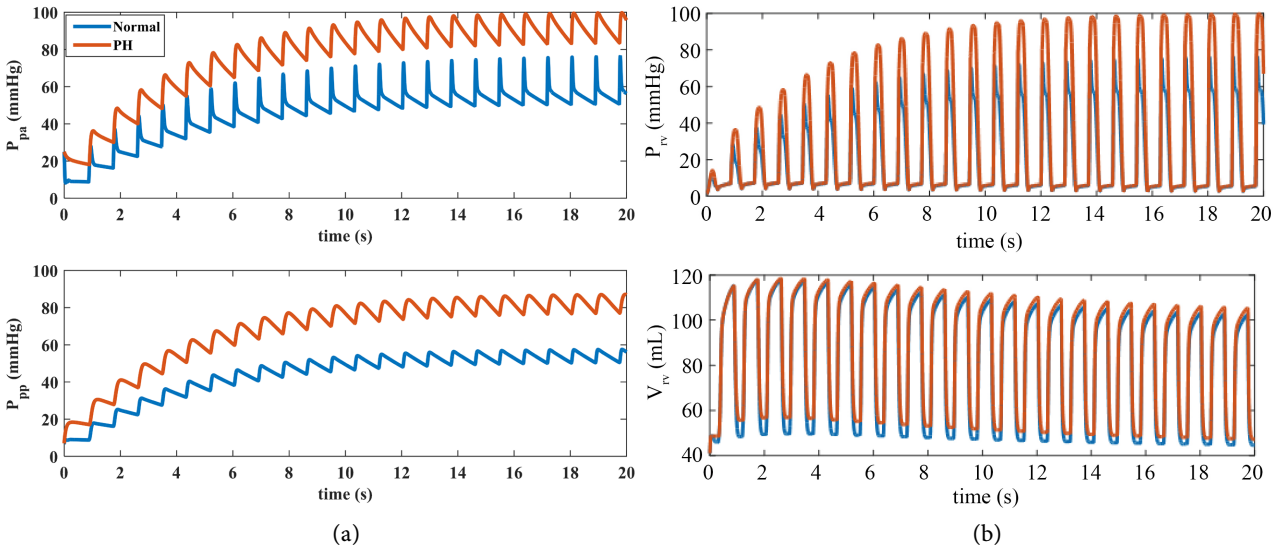

Figure 5. Development of the key pulmonary blood pressures and volume for PHT due to PAS. (a) The pressure signals in the pulmonary arteries and pulmonary peripheral; (b) The pressure signal and the volume signal in the RV.

dropped to 83.8 ± 28.6 mmHg in post-dilation. Moreover, Shikata *et al.* [28] presented a case of PHT pathology and bilateral pulmonary artery stenosis, demonstrating a pulmonary artery pressure of 95/15 (mean 45) mmHg, and a right ventricular pressure of 100/10 (mean 45) mmHg. Furthermore, Tyagi *et al.* [29] examined the case of an aortoarteritis patient with severe proximal right pulmonary artery stenosis. Hemodynamic measurement showed an elevated main pulmonary artery pressure of 80/24 (52) mmHg. On the same, Baerlocher *et al.* [30] evaluated the ratio of RV systolic pressure to aortic pressure of patients with branched PAS and obtained that it was 80.6% and 50.6%, respectively, during pre-dilation and post-dilation of primary balloon angioplasty.

3.2. Results of PHT Caused by Left Ventricular Diastolic Dysfunction

In the case of LVDD, the left ventricular end-diastolic pressure is mathematically elevated by linearly raising the parameters of $A(t)$ and $B(t)$. Simulations are carried out with the modified parameters defined in **Table 4**. The obtained results are dropped in **Figure 6** and **Figure 7**.

Figure 6 exhibits the pressure-volume loops of two heart chambers under normal (blue) and pathological (orange) conditions for the left and right ventricles in the LVDD case. Compared with normal hemodynamic conditions, the established results reveal that the LVDD is manifested directly by the growth of the left ventricular end-diastolic pressure (**Figure 6(a)**). Moreover, it appears in **Figure 6(b)** that event the right ventricular pressure continues to rise until it reaches 70 mmHg. Chatterjee and Massie [31] collected patient data to represent the schematic diagram of P-V relationships in systolic heart failure and in pathologies with diastolic dysfunction. The P-V loop made upward and leftward shifts.

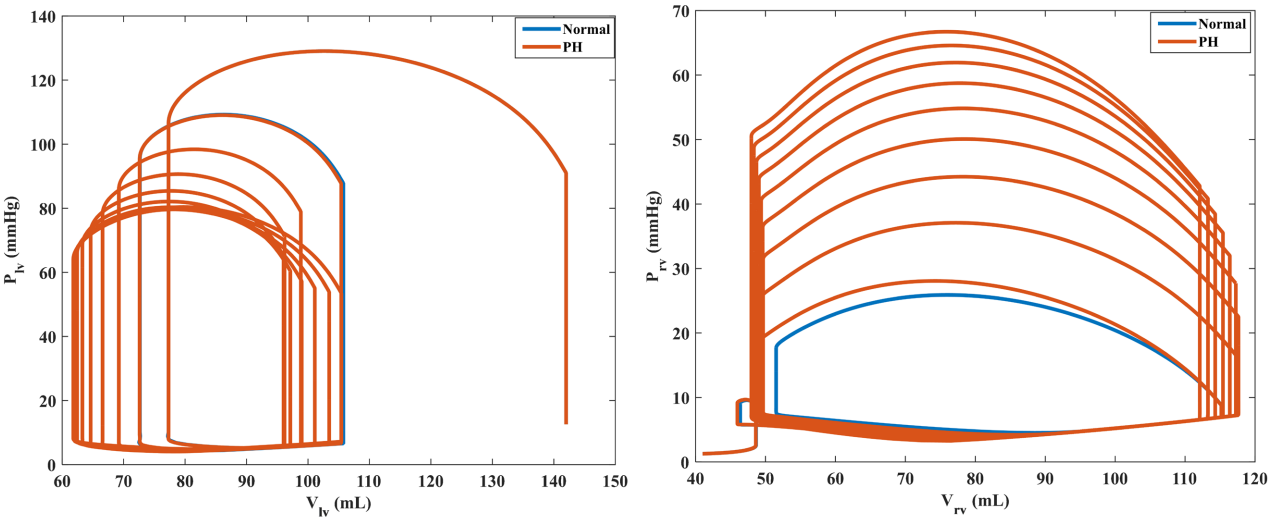

(a) (b)

Figure 6. Pressure-Volume loops of two chambers for PHT due to LVDD. The loops blue are normal and the orange ones are for developing PHT. (a): P-V loops of LV; (b): P-V loops of RV.

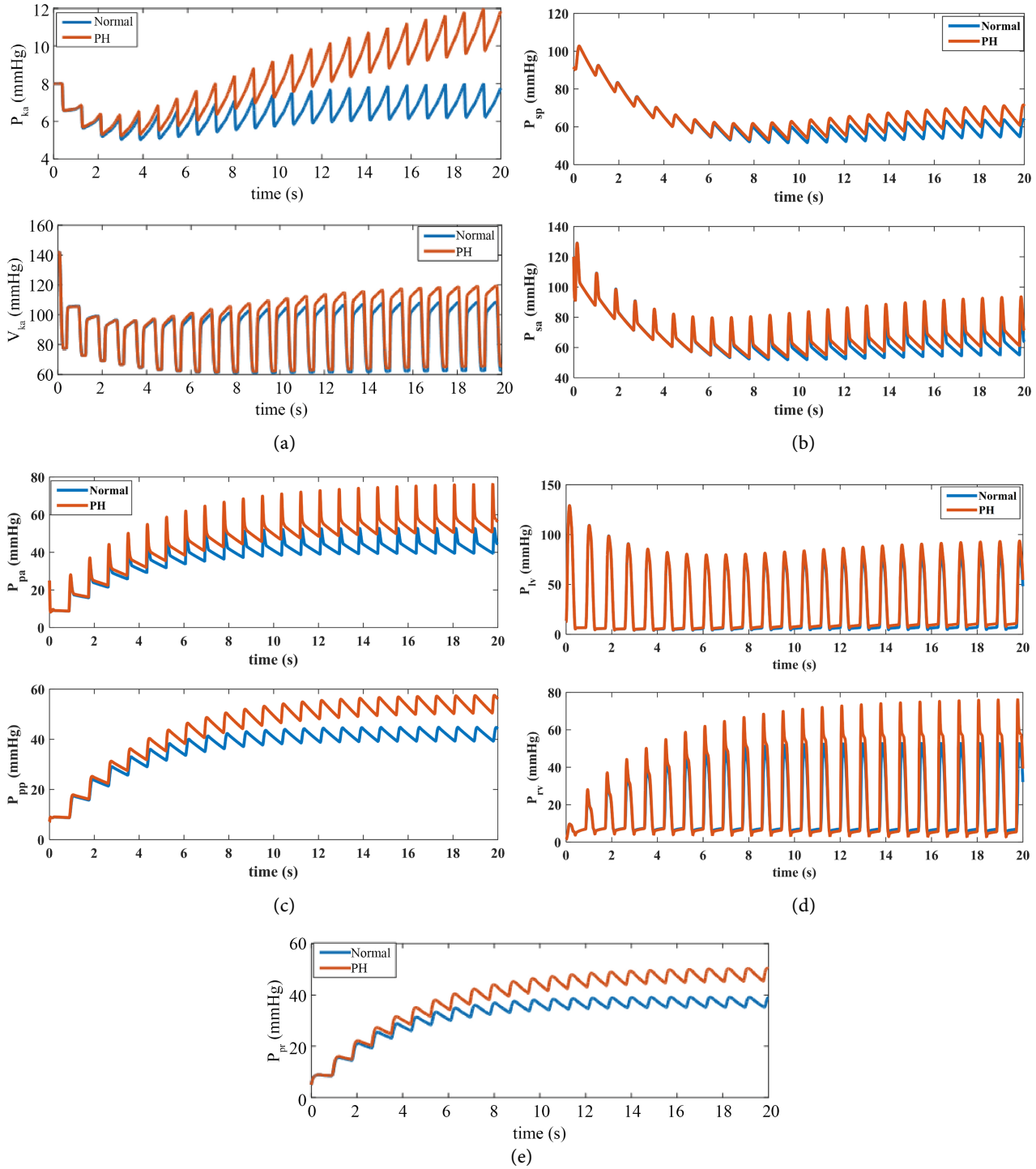

Figure 7. Development of the key pulmonary blood pressures and volume for PHT due to LVDD. (a): The pressure signal and the volume signal in the left atrium; (b): The pressure signals in the systemic arteries and systemic peripheral; (c): The pressure signals in the pulmonary arteries and pulmonary peripheral; (d): The pressure signals in LV and RV; (e): The signal in the pulmonary vein.

Figure 7(a) presents the shape of the pressure and volume signals in the left atrium. Compared to normal situation, it appears that the amplitude of the pressure or volume signal increases in the pathological case of LVDD (orange curves).

Indeed, the left atrium elevates pressure to allow returning of blood to the LV. Long-term blood return is blocked, leading to an accumulation of blood in the left atrium and a consequent increase in its volume. In their clinical work, Kurt *et al*. [32] noted the same observations where the elevation of left atrial volume in patients with diastolic heart failure compared to the normal control group was represented. Due to the development of PHT, the systolic blood pressure of the left atrium continues to increase. This can be explained by the fact that long-term blood flow obstruction changes the function and structure of the left atrium. Moreover, the clinical data established by Melenovsky *et al*. [33] lead to similar results showing that the left atrial pressure and volume in heart failure with preserved ejection fraction increased, and the left atrial stiffness also increased compared to the control group. **Figure 7(b)** displays the decrease to 50mmHg of the symmetric arteries and peripheral pressures, respectively. It can also be seen that growth of systemic artery pressure due to this disease leads directly to the increment of peripheral systemic artery pressure. **Figure 7(c)** presents the time evolution of pulmonary artery pressure (Ppa) and peripheral pulmonary artery pressure (Ppp) allowing to see that increment up to 80mmHg of Ppa due to this disease induces increment up to 60mmHg of peripheral pulmonary artery pressure (orange). On the other hand, it appears from plots of **Figure 7(d)** that the right ventricular pressure continues to rise until it reaches 80 mmHg in the case of developing PHT due to LVDD (orange). Hence, the systolic pressure of the RV would rise to overcome the rise in pulmonary artery pressure. In the case of LVDD, the pressure in the left atrium and pulmonary veins rise (**Figure 7(e)**) leading to an increase in pulmonary artery blood pressure (**Figure 7(c)**).

4. Discussions

The pulmonary vascular resistance (PVR) is an important indicator of pulmonary hemodynamics. We found that increased the PVR can cause PHT. Indeed, the PAS stenosis simulations demonstrate that pulmonary vascular stenosis causes high resistance in the pulmonary arteries, which leads to PHT. For PHT due to LVDD, the PVR may be normal at the onset of PHT, but obviously grows with increasing pulmonary artery pressure.

Given their morphology, physiology and structure, the right and left ventricles must fulfill their functional obligations of pumping blood. The RV can be thought of as a lateral surface that stabilizes additional muscles on the surface of the LV. Because the surface of the RV is thinner than that of the LV, the RV cannot stabilize normal contractile function when the $mPAP$ increases. However, it can adapt well to the growth in blood volume caused by right ventricular reflux.

When the RV afterload increases rapidly, it can cause significant RV expansion. But if the $mPAP$ increases gradually over an extended period, the RV metamorphoses into ventricular hypertrophy by increasing the thickness of one side of the surface to meet the essential contractile force. Thus, the RV can withstand a sustained and significant rise in $mPAP$. The difficulty is that the $mPAP$ generally

grows faster than the adjustment capacity of the RV, so that contractility does not respond to the essential force, resulting in obstacles to the motor function of the RV. In the simulation of two typical cases of PHT examined in this article, it can be seen that the PV loop of the RV gradually changes from normal to a PV loop with very high systolic pressure, and the volume of the RV increases with the development of the disease.

Although both diseases are bad for health, the data obtained show that LVDD affects PHT less than PAS.

We close this discussion by showing some limitations of our work which can lead to new research perspectives. Indeed, the model used in this article does not reflect the complexity of real geometric conditions, thus limiting its innovative contribution to simulation methods. Future studies should propose a modified model that improves the existing unified lumped parameter model allowing it to better reflect cardiovascular dynamics. Furthermore, we did not test the robustness of our model with clinical data from a specific patient. We intend to address this issue in future work by using a multi-scale model in our modeling.

5. Conclusion

In this paper, we set up a lumped parameter model with analog circuit elements to simulate the human circulatory system. Based on this model, the study of two typical cases of PHT due to different pathologies is simulated separately. For a healthy person, it appeared that the LV pressure reached 120 mmHg while remaining lower than the peripheral systemic pressure, likewise the maximum value of the RV pressure remained lower than 25 mmHg. For PHT caused by PAS, compact and inflexible arteries are modeled by increasing resistances. It is shown that increment of pulmonary artery resistance directly induces growth of pulmonary artery blood pressure which is high enough to shift forward the blood flow in the pulmonary circulation. Thus, we established that during PHT, the right ventricular pressure increases leading to a rise of the right ventricular volume. Moreover, we obtained that the systolic blood pressure of the RV rises over 25 mmHg. Concerning PHT due to the LVDD, we have established that the right ventricular pressure continues to rise until it reaches 80 mmHg and the amplitudes of the pressure or volume signal increase. We have also observed that the pressure in the left atrium and pulmonary veins augment leading to an increase in pulmonary artery blood pressure. Moreover, it has appeared from our findings that growth of systemic artery pressure due to this disease leads directly to the increment of peripheral systemic artery pressure. We have noted an increment up to 80 mmHg of the pulmonary artery pressure deals with an elevation up to 60 mmHg of the peripheral pulmonary artery pressure. For each PHT development, the regulation rules of the cardiac chambers, arteries and veins are proposed to adjust to the hemodynamic anomalies. Furthermore, we found that the results established within this work corroborate perfectly with clinical data. These results could be very useful to understand the causes that lead to PHT and the regulation mechanism in the

development of PHT.

Ethics Statement

We, authors of the manuscript entitled "*Modeling the cardiovascular system for the simulation of special cases of pulmonary hypertension*", confirm that this work is original, has not been previously published, in whole or in part, and is not currently under consideration for publication elsewhere.

We have taken all necessary measures to protect the intellectual property relating to this work, and there are no restrictions that would prevent its publication, including those affecting the schedule. Furthermore, we confirm full compliance with the intellectual property regulations of our respective institutions.

Data Access Statement

All data used in this work are cited according to their source. Those not cited are included in the manuscript.

Conflicts of Interest

We confirm that there are no known conflicts of interest between the authors of this manuscript. We acknowledge that the corresponding author, PELAP François Beceau, is the sole point of contact for the editorial process. He is responsible for communication with other authors regarding submission or revisions and final approval of proofs.

We also confirm that we have provided current and correct email addresses accessible to the corresponding author.

References

[1] Colebank, M.J., Umar Qureshi, M. and Olufsen, M.S. (2021) Sensitivity Analysis and Uncertainty Quantification of 1-D Models of Pulmonary Hemodynamics in Mice Under Control and Hypertensive Conditions. *International Journal for Numerical Methods in Biomedical Engineering*, **37**, e3242.

[2] Prins, K.W. and Thenappan, T. (2016) World Health Organization Group I Pulmonary Hypertension. *Cardiology Clinics*, **34**, 363-374. https://doi.org/10.1016/j.ccl.2016.04.001

[3] Barnett, C.F., Alvarez, P. and Park, M.H. (2016) Pulmonary Arterial Hypertension. *Cardiology Clinics*, **34**, 375-389. https://doi.org/10.1016/j.ccl.2016.04.006

[4] D'Alto, M., Dimopoulos, K., Coghlan, J.G., Kovacs, G., Rosenkranz, S. and Naeije, R. (2018) Right Heart Catheterization for the Diagnosis of Pulmonary Hypertension. *Heart Failure Clinics*, **14**, 467-477. https://doi.org/10.1016/j.hfc.2018.03.011

[5] Liu, L.L., Li, L. and Qian, K.X. (2012) Modeling and Simulation of a Fifth-Order Lumped Parameter Cardiovascular System. *Chinese Journal of Biomedical Engineering*, **31**, 13-19.

[6] Xiao, D.W. and Xu, B.L. (2016) Hemodynamic Recovery from Heart Failure with Left Ventricular Assist Device: A Lumped Parameter Simulation. *Beijing Biomedical Engineering*, **35**, Article 367.

[7] Korurek, M., Yildiz, M. and Yuksel, A. (2010) Simulation of Normal Cardiovascular System and Severe Aortic Valve Stenosis Using Equivalent Electronic Model. *The Anatolian Journal of Cardiology*, **10**, 471-478. https://doi.org/10.5152/akd.2010.164

[8] Tsalikakis, D.G., Fotiadis, D.I. and Sideris, D. (2003) Simulation of Cardiovascular Diseases Using Electronic Circuits. 2003 *Computers in Cardiology*, Thessaloniki, 21-24 September 2003, 445-448. https://doi.org/10.1109/cic.2003.1291188

[9] Dolenšek, J., Podnar, T., Runovc, F. and Kordaš, M. (2009) Analog Simulation of Aortic and of Mitral Regurgitation. *Computers in Biology and Medicine*, **39**, 474-481. https://doi.org/10.1016/j.compbiomed.2009.03.009

[10] Luo, C., Ramachandran, D., Ware, D.L., Ma, T.S. and Clark, J.W. (2011) Modeling Left Ventricular Diastolic Dysfunction: Classification and Key Indicators. *Theoretical Biology and Medical Modelling*, **8**, Article No. 14. https://doi.org/10.1186/1742-4682-8-14

[11] Korurek, M., Yildiz, M., Yüksel, A. and Şahin, A. (2011) Simulation of Eisenmenger Syndrome with Ventricular Septal Defect Using Equivalent Electronic System. *Cardiology in the Young*, **22**, 301-306. https://doi.org/10.1017/s1047951111001478

[12] Ratwatte, S., Playford, D., Strange, G., Celermajer, D.S. and Stewart, S. (2024) Prevalence and Prognostic Significance of Pulmonary Hypertension in Adults with Left Ventricular Diastolic Dysfunction. *Open Heart*, **11**, e003049. https://doi.org/10.1136/openhrt-2024-003049

[13] Sahoo, S.K., Khatua, B., Behera, S.K., Bhol, D.R. and Satpathy, P. (2024) Pulmonary Arterial Hypertension in Children with Sickle Cell Anaemia. *European Journal of Cardiovascular Medicine*, **14**, 440-443.

[14] Tang, H., Gao, J. and Park, Y. (2013) Heart Valve Closure Timing Intervals in Response to Left Ventricular Blood Pressure. *Journal of Biomedical Science and Engineering*, **6**, 65-75.

[15] Tang, H., Dai, Z., Wang, M., Guo, B., Wang, S., Wen, J., *et al*. (2020) Lumped-Parameter Circuit Platform for Simulating Typical Cases of Pulmonary Hypertensions from Point of Hemodynamics. *Journal of Cardiovascular Translational Research*, **13**, 826-852. https://doi.org/10.1007/s12265-020-09953-y

[16] Ursino, M. (1998) Interaction between Carotid Baroregulation and the Pulsating Heart: A Mathematical Model. *American Journal of Physiology-Heart and Circulatory Physiology*, **275**, H1733-H1747. https://doi.org/10.1152/ajpheart.1998.275.5.h1733

[17] Frolov, S.V., Sindeev, S.V., Lischouk, V.A., Gazizova, D.S., Liepsch, D. and Balasso, A. (2016) A Lumped Parameter Model of Cardiovascular System with Pulsating Heart for Diagnostic Studies. *Journal of Mechanics in Medicine and Biology*, **17**, Article 1750056. https://doi.org/10.1142/s0219519417500567

[18] Sutera, S.P. and Skalak, R. (1993) The History of Poiseuille's Law. *Annual Review of Fluid Mechanics*, **25**, 1-20. https://doi.org/10.1146/annurev.fl.25.010193.000245

[19] Qin, L., Zhang, H.-L., Liu, Z.-H., *et al*. (2009) Percutaneous Transluminal Angioplasty and Stenting for Pulmonary Stenosis Due to Takayasu's Arteritis: Clinical Outcome and Four-Year Follow-Up. *Clinical Cardiology*, **32**, 639-643. https://doi.org/10.1002/clc.20665

[20] Lankhaar, J., Westerhof, N., Faes, T.J.C., Marques, K.M.J., Marcus, J.T., Postmus, P.E., *et al*. (2006) Quantification of Right Ventricular Afterload in Patients with and without Pulmonary Hypertension. *American Journal of Physiology-Heart and Circulatory Physiology*, **291**, H1731-H1737. https://doi.org/10.1152/ajpheart.00336.2006

[21] Lankhaar, J.-W., Westerhof, N., Faes, T.J.C., Tji-Joong Gan, C., Marques, K.M., Boonstra, A., *et al*. (2008) Pulmonary Vascular Resistance and Compliance Stay Inversely Related during Treatment of Pulmonary Hypertension. *European Heart Journal*, **29**, 1688-1695. https://doi.org/10.1093/eurheartj/ehn103

[22] Acosta, S., Puelz, C., Rivière, B., Penny, D.J., Brady, K.M. and Rusin, C.G. (2017) Cardiovascular Mechanics in the Early Stages of Pulmonary Hypertension: A Computational Study. *Biomechanics and Modeling in Mechanobiology*, **16**, 2093-2112. https://doi.org/10.1007/s10237-017-0940-4

[23] Shang, X., Xiao, S., Dong, N., Lu, R., Wang, L., Wang, B., *et al*. (2017) Assessing Right Ventricular Function in Pulmonary Hypertension Patients and the Correlation with the New York Heart Association (NYHA) Classification. *Oncotarget*, **8**, 90421-90429. https://doi.org/10.18632/oncotarget.19026

[24] Sagawa, K., Sunagawa, K. and Maughan, W.L. (1985) Ventricular End-Systolic Pressure Volume Relations. In: *The Ventricle*, Springer, 79-103. https://doi.org/10.1007/978-1-4613-2599-4_4

[25] Zile, M.R., Baicu, C.F. and Gaasch, W.H. (2004) Diastolic Heart Failure—Abnormalities in Active Relaxation and Passive Stiffness of the Left Ventricle. *New England Journal of Medicine*, **350**, 1953-1959. https://doi.org/10.1056/nejmoa032566

[26] Vonk Noordegraaf, A., Westerhof, B.E. and Westerhof, N. (2017) The Relationship between the Right Ventricle and Its Load in Pulmonary Hypertension. *Journal of the American College of Cardiology*, **69**, 236-243. https://doi.org/10.1016/j.jacc.2016.10.047

[27] Lock, J.E., Castaneda-Zuniga, W.R., Fuhrman, B.P. and Bass, J.L. (1983) Balloon Dilation Angioplasty of Hypoplastic and Stenotic Pulmonary Arteries. *Circulation*, **67**, 962-967. https://doi.org/10.1161/01.cir.67.5.962

[28] Shikata, H., Sakamoto, S., Ueda, Y., Tsuchishima, S., Matsubara, T., Nishizawa, H., *et al*. (2004) Reconstruction of Bilateral Branch Pulmonary Artery Stenosis Caused by Takayasu's Aortitis. *Circulation Journal*, **68**, 791-794. https://doi.org/10.1253/circj.68.791

[29] Tyagi, S., Mehta, V., Kashyap, R. and Kaul, U.A. (2004) Endovascular Stent Implantation for Severe Pulmonary Artery Stenosis in Aortoarteritis (Takayasu'S Arteritis). *Catheterization and Cardiovascular Interventions*, **61**, 281-285. https://doi.org/10.1002/ccd.10741

[30] Baerlocher, L., Kretschmar, O., Harpes, P., Arbenz, U., Berger, F. and Knirsch, W. (2007) Stent Implantation and Balloon Angioplasty for Treatment of Branch Pulmonary Artery Stenosis in Children. *Clinical Research in Cardiology*, **97**, 310-317. https://doi.org/10.1007/s00392-007-0631-8

[31] Chatterjee, K. and Massie, B. (2007) Systolic and Diastolic Heart Failure: Differences and Similarities. *Journal of Cardiac Failure*, **13**, 569-576. https://doi.org/10.1016/j.cardfail.2007.04.006

[32] Kurt, M., Wang, J., Torre-Amione, G. and Nagueh, S.F. (2009) Left Atrial Function in Diastolic Heart Failure. *Circulation*: *Cardiovascular Imaging*, **2**, 10-15. https://doi.org/10.1161/circimaging.108.813071

[33] Melenovsky, V., Hwang, S., Redfield, M.M., Zakeri, R., Lin, G. and Borlaug, B.A. (2015) Left Atrial Remodeling and Function in Advanced Heart Failure with Preserved or Reduced Ejection Fraction. *Circulation*: *Heart Failure*, **8**, 295-303. https://doi.org/10.1161/circheartfailure.114.001667